Boekhout et al., Supplemental Figure S1

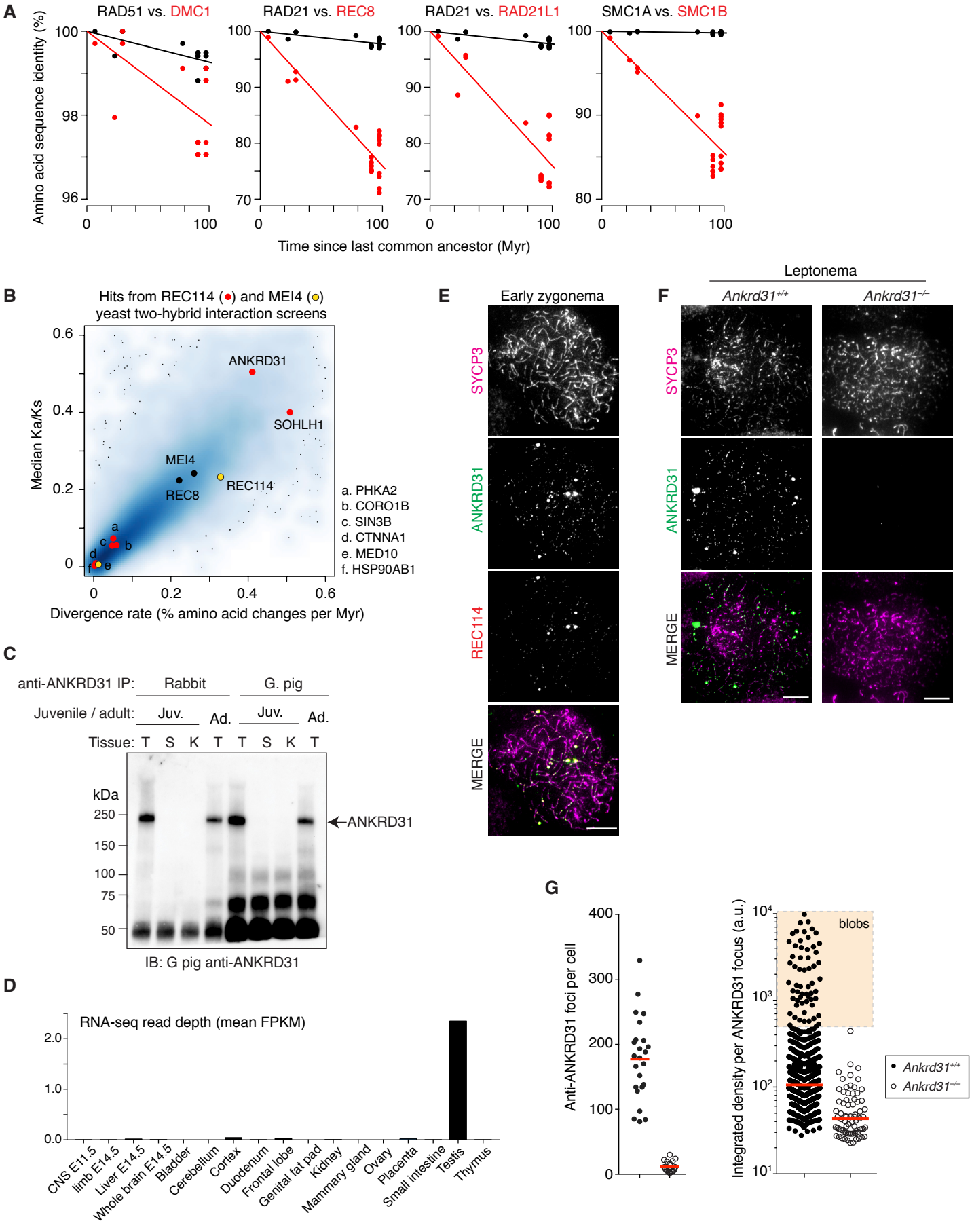

Figure S1. Identification and characterization of *Ankrd31*, related to Figure 1.
(A) Rapid divergence as a signature of meiotic proteins. Meiotic factors are often rapidly evolving (Swanson and Vacquier, 2002; Keeney, 2008). Consistent with this, meiosis-specific proteins typically show more rapid sequence divergence than their more ubiquitously expressed paralogs. For example, the meiotic DNA strand exchange protein DMC1 and the meiotic cohesin subunits REC8, RAD21L, and SMC1β have diverged more than their paralogs that function in all cells (RAD51, RAD21, and SMC1α). Graphs show amino acid sequence identity as a function of time since last common ancestor for pairwise comparisons of orthologs in different mammalian species for either a meiosis-specific protein (red) or its ubiquitously expressed paralog (black). Species included: *Homo sapiens, Pan troglodytes, Maccaca mulatta, Canis familiaris, Bos taurus, Mus musculus,* and *Rattus norvegicus*. Lines are least squares fits with intercepts set at 100% identity. Note the differences in y axes: the trend of more rapid divergence of the meiotic paralog is true regardless of overall rate of sequence divergence for the specific protein type. Even for the relatively highly conserved proteins DMC1 and RAD51, the meiotic version is more rapidly diverging.
(B) Plots of Ka/Ks (ratio of the number of nonsynonymous substitutions per non-synonymous site to the number of synonymous substitutions per synonymous site) vs. amino acid sequence divergence rate within mammals (see STAR Methods). We prioritized hits from the yeast two-hybrid screen by evaluating sequence conservation, reasoning that proteins displaying this signature might be directly involved in meiotic processes. Data for all proteins in the NCBI HomoloGene database (Release 68 (April 2014), https://www.ncbi.nlm.nih.gov/homologene) were plotted using the smoothScatter function in R (blue to gray shading), and overlaid with hits from the yeast two-hybrid screens (red and yellow points). MEI4 and REC8 are shown for comparison. Among the REC114 two-hybrid hits, ANKRD31 and SOHLH1 stood out as having relatively high divergence rates and high Ka/Ks ratios. SOHLH1 is a basic helix-loop-helix transcription factor that regulates germ cell development (Ballow et al., 2006). It is expressed in germline stem cells before meiosis and controls spermatogonial and oocyte differentiation without apparent direct involvement in meiosis per se (Ballow et al., 2006; Shin et al., 2017). We therefore did not explore potential links of SOHLH1 to REC114 function, and instead focused on ANKRD31.
(C) IP and immunoblotting (IB) of ANKRD31 from extracts of testis (T), spleen (S) or kidney (K) from 17-dpp juveniles or testis from adult, using antisera raised in the indicated species. Lower molecular weight bands (100 kDa and below) are independent of tissue origin, they differ depending on which antiserum was used for IP, and they are much more prominent when immunoblotting antibody (anti-guinea pig) matched species for antiserum used for IP. Therefore, these bands are presumably from immunoglobulin and other proteins in the IP antiserum.
(D) *Ankrd31* RNA-seq read depth in various tissues (FPKM, fragments per kb per million reads).
(E) ANKRD31 localizes to chromatin. A wild-type spermatocyte at early zygonema is shown (intermediate stage between spermatocytes shown in Figure 1F).
(F,G) Specificity of the guinea pig anti-ANKRD31 antiserum. Representative leptotene spreads are shown at equivalent exposures in F. Focus numbers per cell and immunofluorescence intensities per focus for cells at early zygonema are shown in G. The focus counts from wild type are reproduced from Figure 1G to aid comparison. The tan-shaded region in G indicates where the heavily stained blobs fall in the intensity plot. The ANKRD31 antibody gave much fewer foci in the *Ankrd31*$^{-/-}$ mutant (11.6 on average, compared to 177.5 in wild type) and these tended to be fainter (median intensity 43.2 in *Ankrd31*$^{-/-}$, compared to 105.8 in wild type).
Scale bars in E, F are 10 μm.

A

Parents' *Ankrd31* genotypes (female × male)	Offspring's *Ankrd31* genotype		
	+/+	+/–	–/–
+/– × +/–	98 (26.6%)	170 (46.2%)	100 (27.2%)
–/– × +/–		96 (48.5%)	102 (51.5%)

B

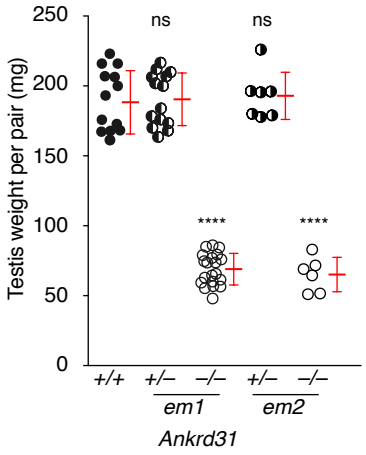

C

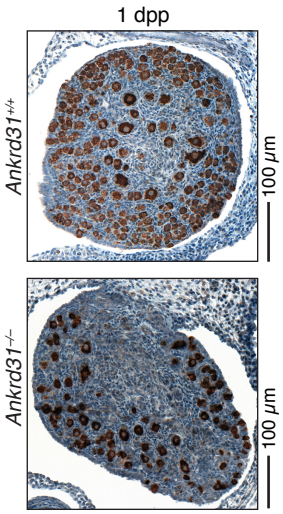

Figure S2. Compromised fertility of *Ankrd31*$^{-/-}$ mutants, related to Figure 2.
(A) Mendelian segregation of the *Ankrd31* frameshift mutation.
(B) Quantification of adult testis weights from mice heterozygous or homozygous for the *Ankrd31*^{em2} allele. Data for wild type and mice heterozygous for the *Ankrd31*^{em1} allele are reproduced from Figure 2A for comparison (red lines, mean ± s.d.). The results of two-tailed t tests for comparison to wild type are indicated: ns, not significant ($p > 0.05$); ****, $p \leq 0.0001$.
(C) Representative ovary sections from newborn animals immunostained for MVH to mark oocytes (brown stain).

Boekhout et al., Supplemental Figure S3

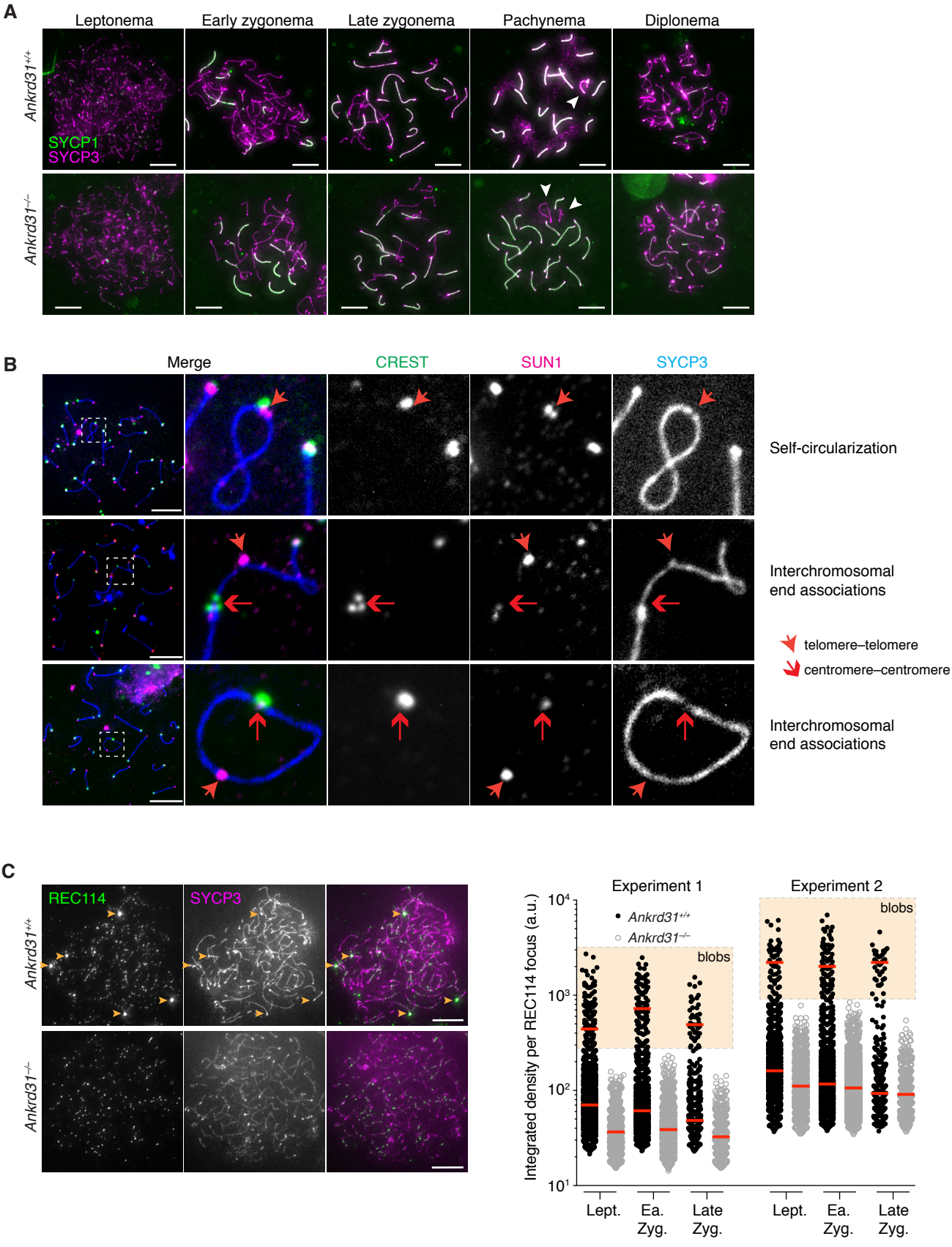

Figure S3. Synaptic defects and altered REC114 focus formation in *Ankrd31*$^{-/-}$ spermatocytes, related to Figure 3.

(A) Meiotic progression in wild-type and mutant spermatocytes. Chromosome spreads were immunostained for SYCP1 and SYCP3. Arrowheads indicate sex chromosomes.

(B) Additional examples of chromosome structure abnormalities observed at elevated frequency in pachytene and pachytene-like spermatocytes from *Ankrd31*$^{-/-}$ mutants.

(C) REC114 focus intensity in *Ankrd31*$^{-/-}$ spermatocytes. At left, additional views are provided of the same cells shown in Figure 3D. Arrowheads indicate REC114 blobs, presumably on mo-2-containing regions, including the PAR. At right are plots of integrated REC114 focus intensities for two independent experiments. The tan-shaded regions indicate where the heavily stained blobs fall in the plots. The graph in Figure 3D summarizes the data from Experiment 1. Red lines indicate medians calculated separately for blobs and smaller foci.

Scale bars in all panels represent 10 μm.

Boekhout et al., Supplemental Figure S4

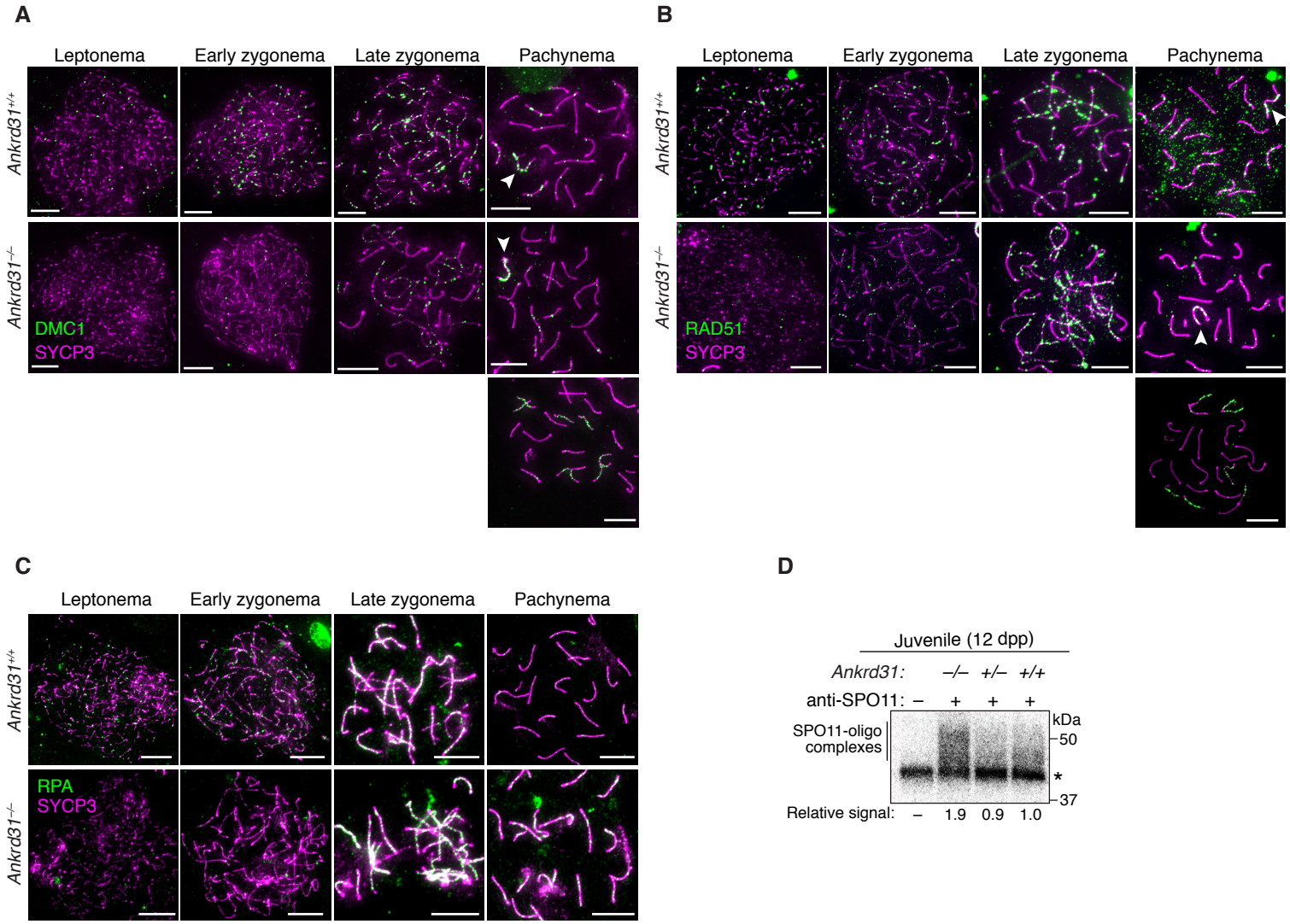

Figure S4. Dysregulated recombination in the absence of ANKRD31, related to Figures 3 and 4.
(A) Altered numbers and timing of recombination foci. Additional images of DMC1 staining at different stages are shown. The early zygotene cells are reproduced from Figure 3E to facilitate comparison. Arrowheads on pachytene images indicate sex chromosomes. For the *Ankrd31*$^{-/-}$ mutant, a pachytene cell with normal-looking synapsis is shown, along with an example of a cell with autosomal asynapsis.
(B) RAD51 immunostaining, as in panel A.
(C) RPA immunostaining using antibodies to the RPA2 subunit, as in panel A.
(D) Example of an autoradiograph of SPO11-oligo complexes immunoprecipitated from juvenile testis extracts, radiolabeled with terminal transferase and [α^{32}P] dCTP, and separated by SDS-PAGE. Asterisk indicates nonspecific labeling. Quantified levels of radioactive signals were background-corrected and normalized to wild type. Unlike quantification in adults, the measurements in juveniles were highly variable, ranging from unchanged in some mice to nearly four fold elevated in others. The reason for this variability is unknown, but we note that even relatively small differences in developmental timing might contribute because the cytological data indicate that DSBs continue to form in the mutant as prophase I progresses. Possible sources of developmental variation could include pre- and postnatal nutrition (e.g., from different litter sizes or maternal nurturing behavior) or small variation in the time between birth and tissue harvest. Importantly, however, the juvenile samples show no evidence of a decrease in SPO11-oligo complexes, which is what would have been predicted if the reduction in recombination foci in leptotene and zygotene cells was because of a decrease in total DSBs. Thus, the juvenile data reinforce the conclusion from the adult data that there is a disconnect between the cytological and molecular assays for DSBs.

Boekhout et al., Supplemental Figure S5

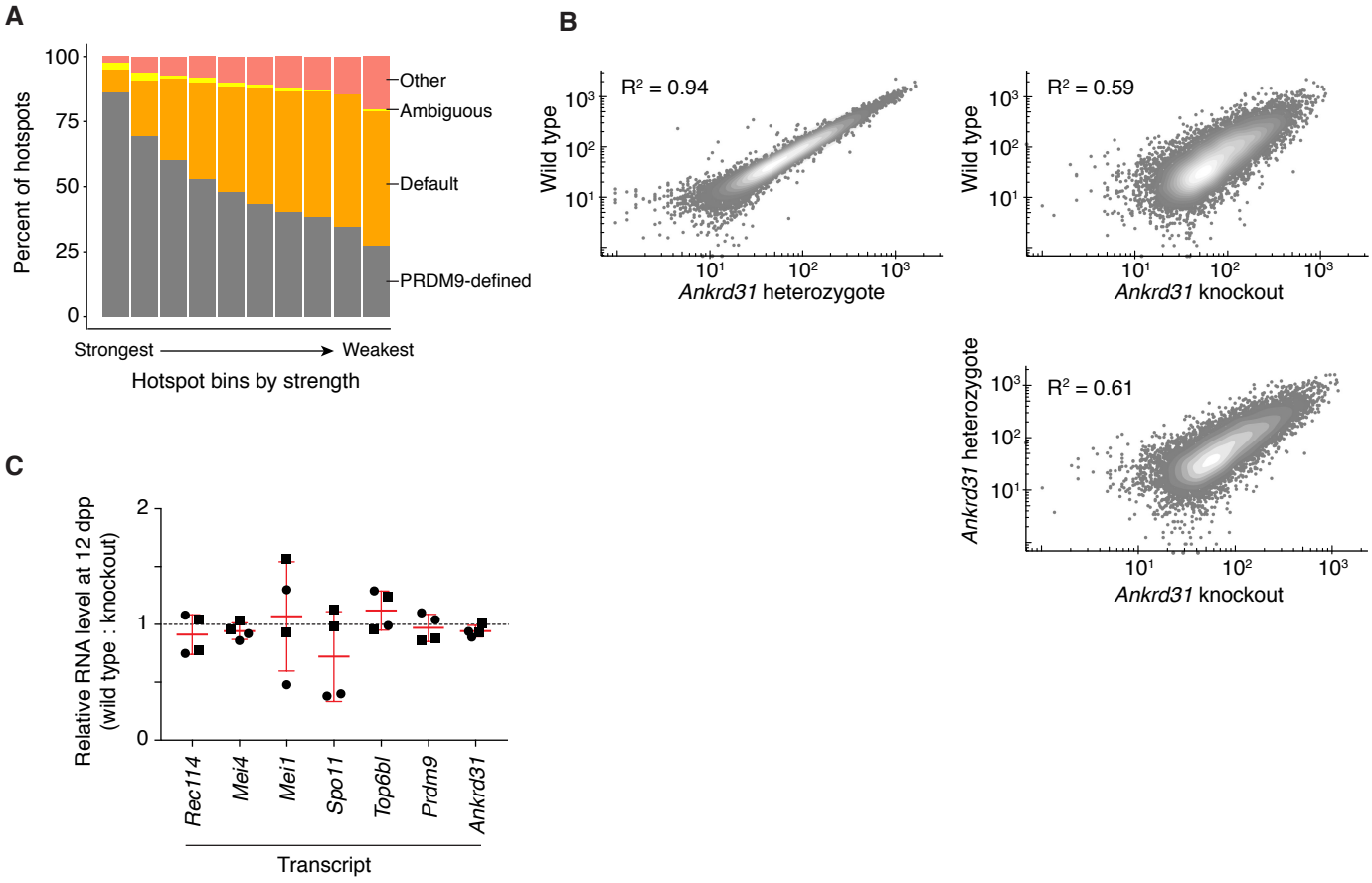

Figure S5. DSB distributions in *Ankrd31*$^{-/-}$ males, related to Figure 5.
(A) Overlaps with PRDM9-defined and default hotspots. Hotspots called in the *Ankrd31*$^{-/-}$ juvenile SSDS map were split into ten bins by strength and scored for overlap with hotspots called from other datasets. “Ambiguous” sites are a hotspot in both B6 wild-type mice and in *Prdm9*$^{-/-}$ mice. “Other” sites are found in neither.
(B) SSDS strength comparisons among strains at PRDM9-defined DSB hotspots (density gradient; grey (low) to white (high)).
(C) *Prdm9* transcript levels are unaltered in *Ankrd31*$^{-/-}$ mutants. RT-qPCR was carried out on RNA extracted from wild-type or mutant animals at 12 dpp. Two primer pairs were used for each gene (filled circles and squares, respectively), for two independent experiments. Red error bars indicate pooled means ± s.d. Interestingly, *Ankrd31* transcript levels were also not reduced, suggesting that the mutant mRNA is not subject to substantial levels of nonsense-mediated decay, at least at this stage in development. *Spo11* transcripts were lower in two samples but not the others, so alterations in SPO11 expression are unlikely to be the cause of *Ankrd31*$^{-/-}$ phenotypes.

Boekhout et al., Supplemental Figure S6

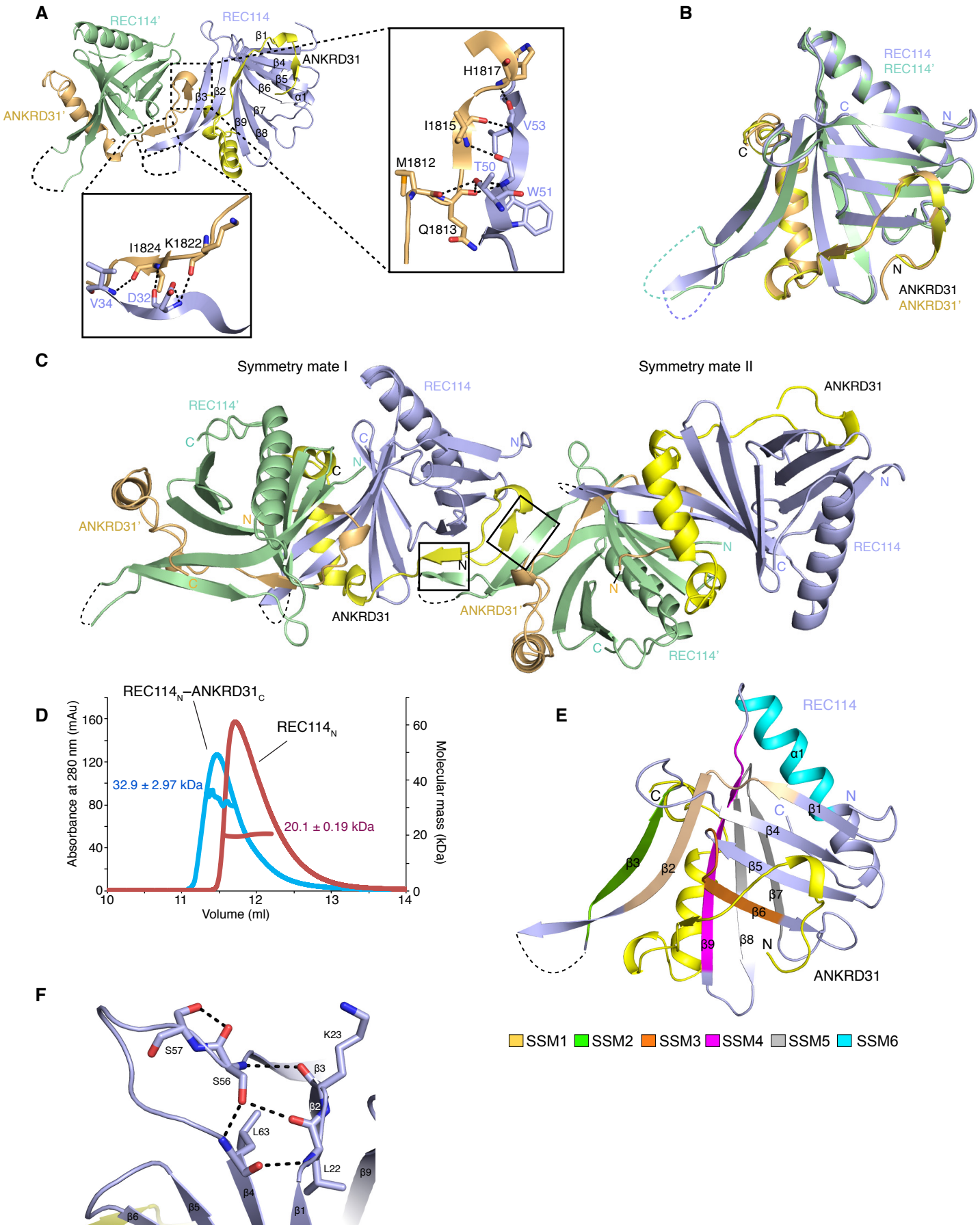

Figure S6. REC114$_N$–ANKRD31$_C$ complexes and conservation of REC114$_N$ structural features, related to Figures 6 and 7.

(A) Detailed contacts between two REC114$_N$-ANKRD31$_C$ heterodimers in the asymmetric unit. Note that these contacts are distinct from the dimer interface in an independent crystal structure of the REC114 PH domain alone (Kumar et al., 2018). The latter interface does not appear to be occluded by binding to the ANKRD31$_C$ peptide in our structure, suggesting that the interaction reported by Kumar et al. (2018) is a relatively weak one that may be due to crystal packing.

(B) Superposition of two REC114$_N$-ANKRD31$_C$ heterodimers in the asymmetric unit.

(C) Interactions of two adjacent symmetry mate REC114$_N$–ANKRD31$_C$ dimers in the crystal lattice. Key contacts contributing to crystal packing are in black boxes.

(D) Molecular weights of REC114$_N$ alone and of the REC114$_N$–ANKRD31$_C$ complex measured by size exclusion chromatography with in-line multi-angle light scattering (SEC-MALS). Observed molecular weights are comparable with estimates for monomeric REC114$_N$ (20.1 kDa measured versus 17.3 kDa predicted) and REC114$_N$–ANKRD31$_C$ heterodimer (32.9 kDa measured versus 23.3 kDa predicted). These measurements reinforce that contacts between heterodimers are likely due to crystal packing.

(E) Mapping of SSMs to the REC114$_N$-ANKRD31$_C$ heterodimer structure. Color code for SSMs is the same as in Figure 6E.

(F) Detailed interactions involving S56 in REC114$_N$.

Table S1. Primers. Related to STAR Methods

	Forward (5′→3′)	Reverse (5′→3′)
pGAD-ANKRD31 cloning primers		
1-376	GGAGGCCAGTGAATTCatggagaacggtgccgaggc	CACCCGGGTGGAATTCctgggtagaggtatttttttatgggatctga
367-837	GGAGGCCAGTGAATTCtcagatcccataaaaaatacctctacccag	CACCCGGGTGGAATTCtgagctattgtttccaagggacttatatggg
829-1153	GGAGGCCAGTGAATTCccatataagtcccttggaaacaatagctca	CACCCGGGTGGAATTCttgtgttcacgccttggctgca
1147-1837	GGAGGCCAGTGAATTCtgcagccaaggcgtgaacacaa	CACCCGGGTGGAATTCatgagggatggtttgcatcgactc
1810-1857	GGAGGCCAGTGAATTCgagtcgatgcaaaccatccctcat	CACCCGGGTGGAATTCggttaaggtatgcccaccacgcg
pGBK-REC114 cloning primers		
1-65	CATGGAGGCCGAATTCatgtctgaagcgggaaatgtgg	GGATCCCCGGGAATTCgaggacaagactcccggattcttc
1-76	CATGGAGGCCGAATTCatgtctgaagcgggaaatgtgg	GGATCCCCGGGAATTCggaaatgaagaagtgacctgatacaac
1-147	CATGGAGGCCGAATTCatgtctgaagcgggaaatgtgg	GGATCCCCGGGAATTCgctcctgaacggtgacgtactg
30-116	CATGGAGGCCGAATTCctcttggacaacgtgggg	GGATCCCCGGGAATTCaaacattcggctcttgttctttattgt
68-147	CATGGAGGCCGAATTCgttgtatcaggtcacttcttcatttcc	GGATCCCCGGGAATTCgctcctgaacggtgacgtactg
68-227	CATGGAGGCCGAATTCgttgtatcaggtcacttcttcatttcc	GGATCCCCGGGAATTCcaattcttctgttccccatgaagagcct
141-260*	CATGGAGGCCGAATTCcagtacgtcaccgttcaggagc	GGATCCCCGGGAATTCttcagttccttagttgcatacatgtgc
219-260*	CATGGAGGCCGAATTCggctcttcatggggaacagaagaattgg	GGATCCCCGGGAATTCttcagttccttagttgcatacatgtgc
full length	GGAATTCCATATGATGTCTGAAGCGGGAAATGTGG	GGCGCGGAATTCTTAGTTTCTCAACCCTGTAATC
pGBK-MEI4 cloning primers		
Full length	GGCGAGCCATATGATGGATATTCAGCCATGGTATTTG	GGCGAGCCATATGATGGATATTCAGCCATGGTATTTG
RT-qPCR primers		
Ankrd31-1	ATAATGCAGGTTGGACTCCCC	CCGCAGAAGCACCATGTAAAG
Ankrd31-2	AGCCAAGTTACGATGGGTGG	CGCATCATGCAGGGGAGTAATC
Rec114-1	CGAAGTCTCCCAGTGGTCTCTG	ACGATCGTGAGGACAAGACTCC
Rec114-2	TCAGTGACACATCGAGCTCAGTC	CCACCTCTTCCACAAATGCTGG
Mei4-1	CGGAGGGACAAAAGCCAAGATG	TTCCATGTGGACTCCTTCTGGG
Mei4-2	GGAGCCATCGATCAGGATCAAG	GATGCTGTGATCCATGTGTGC
Top6bl-1	CACTCTTGTTGTGGGCTTCCAG	AGTCAGTGTCAGTTCTCCCAGC
Top6bl-2	CCAGAACACCAAAGACCAGCAC	TCTCTTGCTGAGCCCAGAACTC
Spo11-1	TCCAGTGTACCTGTAGTGCCAC	GGACATCCTGCTGCAGAAGTTG
Spo11-2	CCCACTGACAAAGCATGACCAG	AGTCTGCCATCATCTCCAGCTC
Prdm9-1	CGATCCCAGTAGACGGTCTTGG	GAAAGCTGGTCTAGGGGCTC
Prdm9-2	ACAAGTCAGTCCTCCTTGGGTG	AAGGGAGGACACTGGTTTCTGG
Mei1-1	ATGAGGATGTCAAGGTGGGTGG	TCATCTGCACCAAGGACAGGAG
Mei1-2	TTCACCCTCTTGGATGCTGGAG	GAGCTGACAGGTCAACCAAAGC
B2M	ACACTGAATTCACCCCCACTGA	CGATCCCAGTAGACGGTCTTGG
Genotyping primers		
ANKRD31-A/ ANKRD31-B	CTTCTGAATATAGAATTATAAAATTCTGAGAAG	CTTGTAATTAGTAATTTGCCACAG
16G008/ 16G011	ACCCAGGTTTCATATATGCTAATGGTACCC	TGCCACAGATAGCAGTTCCATCTTTTG

* Reverse primer is in 3’ UTR.

Table S2. Antibodies. Related to STAR Methods

Primary Antibodies

Target	Dilution for IF	Dilution for immunoblot	Host Species	Supplier	Catalog number
γH2AX	1:1000	n/a	Rabbit	Santa Cruz	sc-101696
DMC1	1:100	n/a	Rabbit	Santa Cruz	sc-22768
MLH1	1:25	n/a	Mouse	BD-Pharmigen	51-1327GR
RPA (H-100)	1:75	n/a	Rabbit	Santa Cruz	sc-28709
RAD51	1:100	n/a	Rabbit	Merck Millipore	PC130
SYCP3 (D-1)	1:400	n/a	Mouse	Santa Cruz	sc-74569
SYCP3 (M-14)	1:200	n/a	Goat	Santa Cruz	sc-20845
REC114	1:100	n/a	Rabbit	Stanzione et al., 2016	n/a
ANKRD31	1:200	1:4000	Guinea Pig	This study	n/a
ANKRD31	1:200	n/a	Rabbit	This study	n/a
CREST	1:500	n/a	Human	Immunovision	HCT-0100
SUN1	1:50	n/a	Rabbit	Abcam	ab103021
	Dilution for IP / immunoblot				
SPO11-180	1:2000		Mouse	MSKCC Antibody and Bioresource Core Facility	n/a
	Histology				
VASA/MVH/DDX4	0.17 µg/ml		Rabbit	Abcam	ab13840
	ChIP				
Histone H3K4me3	n/a		Rabbit	Abcam	ab8580

Secondary Antibodies

Target	Dilution for IF	Fluorophore	Host Species	Supplier	Catalog number
anti Goat	1:400	Alexa-350	Donkey	Mol Probes	A-21081
anti Guinea pig	1:400	Alexa-488	Goat	Mol Probes	A-11073
anti Mouse	1:400	Alexa-594	Donkey	Life Technologies	A21203
anti Mouse	1:400	Alexa-594	Goat	Mol Probes	A-11005
anti Rabbit	1:400	Alexa-488	Goat	Invitrogen	A11034
anti Rabbit	1:400	Alexa-488	Donkey	Thermofisher Scientific	R37118